

RESEARCH

Open Access



# Development of quantitative and continuous measure for severity degree of Alzheimer's disease evaluated from MRI images of 761 human brains

Sangyeol Kim<sup>1,2\*†</sup>, Seongjun Park<sup>3†</sup>, Iksoo Chang<sup>1,2,4\*</sup> and the Alzheimer's Disease Neuroimaging Initiative

<sup>†</sup>Sangyeol Kim and Seongjun Park have contributed equally to this work

\*Correspondence: sykim@dgist.ac.kr; iksoochang@dgist.ac.kr

<sup>1</sup> Department of Brain Sciences, Daegu Gyeongbuk Institute of Science and Technology, Daegu, Korea

<sup>2</sup> Brain Sciences Research Institute, Daegu Gyeongbuk Institute of Science and Technology, Daegu, Korea

<sup>3</sup> Department of Emerging Materials Science, Daegu Gyeongbuk Institute of Science and Technology, Daegu, Korea

<sup>4</sup> Supercomputing Bigdata Center, Daegu Gyeongbuk Institute of Science and Technology, Daegu, Korea

## Abstract

**Background:** Alzheimer's disease affects profoundly the quality of human behavior and cognition. The very broad distribution of its severity across various human subjects requires the quantitative diagnose of Alzheimer's disease beyond the conventional tripartite classification of cohorts such as cognitively normal (CN), mild cognitive impairment (MCI), Alzheimer's disease (AD). The unfolding of such broad distributions by the quantitative and continuous degree of AD severity is necessary for the precise diagnose in the cross-sectional study of different stages in AD.

**Results:** We conducted the massive reanalysis on MRI images of 761 human brains based on the accumulated bigdata of Alzheimer's Disease Neuroimaging Initiative. The score matrix of cortical thickness profile at cortex points of subjects was constructed by statistically learning the cortical thickness data of 761 human brains. We also developed a new and simple algebraic predictor which provides the quantitative and continuous degree of AD severity of subjects along the scale from 0 for fully CN to 1 for fully AD state. The mathematical measure of a new predictor for the degree of AD severity is presented based on a covariance correlation matrix of cortical thickness profile between human subjects. One can remove the uncertainty in the determination of different stages in AD by the quantitative degree of AD severity and thus go far beyond the tripartite classification of cohorts.

**Conclusions:** We unfold the nature of broad distribution of AD severity of subjects even within a given cohort by the scale from 0 for fully CN to 1 for fully AD state. The quantitative and continuous degree of AD severity developed in this study would be a good practical measure for diagnosing the different stages in AD severity.

**Keywords:** Alzheimer's disease, Mild cognitive impairment, MRI, Cortical thickness, Bigdata



## Introduction

Alzheimer's disease (AD) profoundly affects human health and behavior. The diagnosis of AD requires not only the identification of cohort that classify different tripartite stages of AD but also the estimation of the severity degree of AD for a given individual [1–5]. The symptoms of AD appear in various forms in the human body, behavior, and cognition, yet the direct anatomical evidences appear in the structural change within the brain [6–11]. Among these evidences is the degradation of the cortical thickness of human brain, which is one of the imprints of AD. Such physical change can be monitored through the neuro-image, for example the magnetic resonance image (MRI) analysis of the brain [12–17]. The anatomical degradation of the cortical thickness becomes more pronounced as the degree of AD severity becomes greater [13, 17].

Given the information of cortical thickness of human brains, previous studies have noted that the person-to-person fluctuations in cortical thickness of an individual may overwhelm the degradation in cortical thickness. In clinical cases, we frequently observed that the average cortical thickness of some cognitively normal people is thinner than that of people with AD, which appears to contrast the conventional view. Also we recognized the ambiguity in what we should do if two different cohorts have a difference in the cortical thickness in brain regions that have little to do with AD. In principle we should construct some good determinants for judging the degree of AD severities of human subjects, but in practice we are confronted with the differences in cortical thickness in regions of the cortex that are unrelated to the pathogenesis of AD. The abundant existence of such unrelated regions is an intrinsic source that increases the uncertainty of the AD determinants and hinders the appropriate construction of good classifier and predictor for AD.

In this study we developed a simple and straightforward algebraic predictor for providing the continuous and quantitative degree of AD severity of human subjects along the scale from 0 for fully CN to 1 for fully AD state. Instead of dealing with all 327,684 vertices point on the whole cortex of a human brain, we strived to overcome the before mentioned obstacles and demonstrated that the consideration of a few hundred essential vertices were enough for distinguishing CN, MCI, AD cohorts each other. With cortical thickness data at these essential vertices of 1006 human brain images for control and 510 human brain images for independent validation, we defined the machined-learned score matrix and the covariance correlation matrix between human subjects as a new set of classifier and predictor for AD severity.

Over the past decade, there have been developments in diagnosing CN/MCI/AD with various deep learning techniques, such as Deep Neural Network and Convolution Neural Network [18]. And the accuracy of the diagnosis by deep learning techniques has already reached a significant level. Raju et al. [19] showed 97.77% accuracy for ADNI 465 subjects using the Convolution Neural Network, and Albright [20] showed 86.6% accuracy for ADNI 1737 subjects using Deep Neural Network. Our results may not be satisfactory enough if we only compare the accuracy of the diagnosis. However, we have a significant advantage of discovering ROI in an intuitive way, performing diagnostics based on it, and providing severity degree for individual patients.

Our study suggests that unlike the conventional view that the degradation of the cortical thickness of human brain was sole responsible for AD, the singular valued

decomposition analysis of the score matrix developed in this study clearly revealed that the simultaneous consideration of both thinner and thicker cortical regions together compared to those of CN are important and very necessary for the precise diagnose of the AD severity. Based on a covariance correlation matrix of cortical thickness profile between human subjects, we could determine the quantitative and continuous degree of AD severity for a given subject even within a given cohort and also tell how much a subject is prone to CN, AD, or positioned at a particular stage in between. This study not only provided a straightforward algebraic determinant to analyzing the cortical thicknesses of human brains but also suggested quantitative measures by which one could estimate both the cohort and the severity degree of AD for a given new subject based on the neuro-images from the structural MRI. The MRI data of a new and larger number of human brains could also be machine-learned into this study in a systematic and robust manner, which would facilitate the better diagnose of AD with the different degree of severity.

## Methods

### Preparation of cortical thickness data from MRI of 1522 human brain images from ADNI

We selected 274 individuals (human subjects) who were identified as CN, 265 individuals with MCI, 125 individuals with AD from the ADNI-2 study of ADNI, and 97 individuals with MCI from the ADNI-GO study of ADNI. A human brain image-data set of 1522 MR images from a total of 761 subjects was constructed, for each of which both 1.2-mm sagittal Magnetization Prepared Rapid Gradient Echo (MPRAGE) and MPRAGE\_SENSE2 images were taken separately. Here, we note that the longitudinal study of AD is beyond the scope of this work. Therefore, we ignore the number of visits of subject required to perform any longitudinal study.

### Partition 1516 MR images of human brains into four groups and determine the essential region-of-interest vertices for each group

We performed the FreeSurfer analysis to obtain the cortical thickness data at 327,684 vertices on the cortex of a human brain [21, 22]. The cortical thickness at each vertex ranges from 0 to 5 mm. After eliminating those vertices at which cortical thickness information was missing for any one of the 1522 MR images of human brains in the ADNI data set, 276,825 common vertices whose cortical thickness values are available for all 1522 MR images were selected for our study. The average cortical thickness over 276,825 vertices for each brain images was evaluated, and we divided 1516 values of average thickness into four groups (A-D) of different windows of average thickness except 6 values of that run out-of-bounds. Demographic characteristics of the average cortical thickness of the four groups are listed in Table 1.

In order to assign subjects from each CN, MCI, and AD cohort into one of the four groups (A-D) of average cortical thickness, we employed the  $Z$  score criteria in selecting the region-of-interest (ROI) vertices and the essential ROI vertices on the cortex at which the distribution of cortical thickness of the CN cohort is distinguished from that of the AD cohort within each group of average cortical thickness. A similar procedure

**Table 1** Demographic characteristics of the groups

	CN	MCI	AD
<i>Group A</i>			
N*	136	155	13
Female (%)	60.3	53.5	30.8
Age, Mean (SD)	72.5 (5.3)	72.1 (5.1)	78.1 (5.0)
<t>†, Mean (SD)	2.4580 (0.0477)	2.4549 (0.0415)	2.4676 (0.0539)
<i>Group B</i>			
N	212	262	67
Female (%)	62.7	43.5	41.8
Age, Mean (SD)	73.0 (5.2)	73.7 (5.3)	76.7 (6.3)
<t>, Mean (SD)	2.3516 (0.0293)	2.3429 (0.0266)	2.3491 (0.0269)
<i>Group C</i>			
N	159	209	84
Female (%)	46.5	34.0	52.4
Age, Mean (SD)	74.0 (5.7)	75.3 (5.8)	76.9 (5.2)
<t>, Mean (SD)	2.2566 (0.0290)	2.2573 (0.0278)	2.2455 (0.0298)
<i>Group D</i>			
N	40	96	83
Female (%)	22.5	35.4	26.5
Age, Mean (SD)	78.1 (6.5)	76.2 (5.7)	77.4 (6.6)
<t>, Mean (SD)	2.1514 (0.0389)	2.1448 (0.0433)	2.1373 (0.0520)

\*Number of MRI images; †Average cortical thickness over the 276,825 vertices. AD Alzheimer’s disease, CN cognitively normal, MCI mild cognitive impairment

is repeated for distinguishing the CN cohort from the MCI cohort and also the MCI cohort from the AD cohort:

$$\begin{aligned}
 Z_p^{CN-MCI} &= \frac{\langle t_{p,h \in CN} \rangle - \langle t_{p,h \in MCI} \rangle}{\sqrt{\frac{\sigma_{p,h \in CN}^2}{n_{p,h \in CN}} + \frac{\sigma_{p,h \in MCI}^2}{n_{p,h \in MCI}}}}, Z_p^{CN-AD} = \frac{\langle t_{p,h \in CN} \rangle - \langle t_{p,h \in AD} \rangle}{\sqrt{\frac{\sigma_{p,h \in CN}^2}{n_{p,h \in CN}} + \frac{\sigma_{p,h \in AD}^2}{n_{p,h \in AD}}}}, \\
 Z_p^{MCI-AD} &= \frac{\langle t_{p,h \in MCI} \rangle - \langle t_{p,h \in AD} \rangle}{\sqrt{\frac{\sigma_{p,h \in MCI}^2}{n_{p,h \in MCI}} + \frac{\sigma_{p,h \in AD}^2}{n_{p,h \in AD}}}}.
 \end{aligned} \tag{1}$$

Here,  $\langle t_{p,h \in k} \rangle$  is the average cortical thickness at a vertex point  $p$  averaged over the subject  $h$  who belongs to the  $k$  (one of CN, MCI, AD) cohort, and  $\sigma_{p,h \in k}$  is its standard deviation, and  $n_{p,h \in k}$  is the number of MR images belonging to the  $k$  cohort. The positive (negative) value of  $Z_p^{CN-AD}$ , for example, indicates that the distribution curve of the average cortical thickness of the CN cohort is right (or left)-shifted compared to that of AD cohort. And the bigger the absolute value of the Z score, the better distinguished the distribution curves of average cortical thickness of the cohorts. In this study, we identified ROI vertices satisfying the absolute value of the Z score larger than 1.5, and essential ROI vertices satisfying much higher cut-off Z scores (Additional file 1: Table S1).

**Construction of a statistical score matrix for classifying subjects into one of CN, MCI, AD cohorts**

Within each group of average cortical thickness, we constructed the statistical score matrix for determining a subject’s cohort as either CN, MCI, or AD [23]. First of all,  $t_{p,h \in k}$  was transformed into the probability distribution matrix  $P_{p,m}^{(k)}$ , which is a probability that the cortical thickness  $t_{p,h \in k}$  at a vertex point  $p$  of the subject in  $k$  cohort is between  $(m - 1)\Delta$  and  $m\Delta$ :

$$P_{p,m}^{(k)} = \frac{\sum_{h \in k} \Theta(t - (m - 1)\Delta) \bullet \Theta(m\Delta - t) \bullet \delta(t - t_{p,h})}{\sum_{h \in k} 1}, m = 1, 2, \dots 30, k = \text{CN, MCI, AD.} \tag{2}$$

Here,  $\Delta = 0.2$  mm, and cortical thickness index  $m$  runs from 1 to 30; this covers the cortical thickness from 0 to 6 mm.  $\delta(x)$  is a Dirac delta function, and  $\Theta(x)$  is a step function where  $\Theta(x < 0) = 0$ ;  $\Theta(x \geq 0) = 1$ . Then, we defined the statistical score matrix  $S_{p,m}^{(k)}$  from  $P_{p,m}^{(k)}$  in the following way:

$$S_{p,m}^{(k)} = -\ln \left[ \frac{Q_{p,m}^{(k)}}{Q_p^{(k)}} \right], Q_{p,m}^{(k)} = \frac{P_{p,m}^{(k)}}{\sum_m P_{p,m}^{(k)}}, Q_p^{(k)} = \frac{\sum_m P_{p,m}^{(k)}}{\sum_p \sum_m P_{p,m}^{(k)}}. \tag{3}$$

Since  $\sum_m P_{p,m}^{(k)} = 1$ ,  $S_{p,m}^{(k)} = -\ln P_{p,m}^{(k)} - \ln \sum_p 1$  and the second term are constants. The value of the statistical score matrix  $S_{p,m}^{(k)}$  varies depending on the cohort  $k$ ; the smaller  $S_{p,m}^{(k)}$  is, the larger  $P_{p,m}^{(k)}$  is.

With this statistical score matrix  $S_{p,m}^{(k)}$ , we employed a strategy for determining to which one of  $k$  cohorts a given subject would belong. First, we evaluated the averaged cortical thickness of a given subject over 276,825 vertices. Second, we assigned this subject to one of four groups (A-D) of average cortical thickness. Third, based on the preselected essential ROI vertices  $p$  for the assigned group, we determined the cortical thickness index  $m'(p)$  at which the cortical thickness at an essential ROI vertex  $p$  is between  $(m - 1)\Delta$  and  $m\Delta$ . Then, for each  $k$  cohort, the total score  $S'_{(k)}$  was calculated by summing up  $S_{p,m'(p)}^{(k)}$  over the preselected essential ROI vertices  $p$  for the assigned group of the average cortical thickness,  $S'_{(k)} = \sum_p S_{p,m'(p)}^{(k)}$ . Lastly, to which  $k$  cohort a given subject would belong was decided by a cohort which gives the minimum score out of  $S'_{(\text{CN})}$ ,  $S'_{(\text{MCI})}$ ,  $S'_{(\text{AD})}$ .

We, however, noted that the accuracy of both  $P_{p,m}^{(AD)}$  and  $S_{p,m}^{(AD)}$  may become unsatisfactory if the number of people in the AD cohort was less than that of the CN cohort and the MCI cohort (Table 1). In order to overcome the unsatisfactory nature of both  $P_{p,m}^{(AD)}$  and  $S_{p,m}^{(AD)}$ , we employed the method of Kernel Density Estimation (KDE); namely, a Dirac delta function  $\delta(t - t_{p,h})$  in the definition of the probability distribution matrix  $P_{p,m}^{(k)}$ , is replaced by a kernel function  $f(t - t_{p,h})$ :

$$f(t - t_{p,h}) = \sum_{l=-4}^4 a_l \delta(t - (t_{p,h} + l\Delta)), \tag{4}$$

$$a_l = 0.5 \operatorname{erf}(0.25 + 0.5|l|) + \frac{a_0}{2} - \sum_{l'=0}^{|l|-1} a_{l'}; \operatorname{erf}(x) = \frac{2}{\sqrt{\pi}} \int_0^x e^{-q^2} dq. \tag{5}$$

Here, the relative ratio among coefficients  $a_l$  is  $a_0 : a_{\pm 1} : a_{\pm 2} : a_{\pm 3} : a_{\pm 4} = 56 : 43 : 21 : 7 : 1$ . The kernel function  $f(t - t_{p,h})$  satisfies  $\int_{-\infty}^{\infty} f(t - t_{p,h}) dt \approx 1$  and the standard deviation  $\sigma_f \approx 1.435$ . Upon subjecting KDE,  $P_{p,m}^{(k)}$  becomes

$$P_{p,m}^{(k)} = \frac{\sum_{h \in k} \Theta(t - (m - 1)\Delta) \bullet \Theta(m\Delta - t) \bullet f(t - t_{p,h})}{\sum_{h \in k} 1}, m = 1, 2, \dots, 30, k = \text{CN, MCI, AD}. \tag{6}$$

In this study, we constructed the statistical score matrix on which KDE was employed and used it for determining to which  $k$  cohort a given subject would belong.

**Construction of a covariance correlation matrix and a predictor for the severity degree of AD**

Within each group of the average cortical thickness, the severity degree of AD for a given subject is estimated by the following strategy. First of all, we transformed the cortical thickness matrix  $t_{p,h}$  at essential ROI vertices  $p$  for a subject  $h$  into the normalized matrix  $t'_{p,h}$  such that

$$t'_{p,h} = \frac{t_{p,h} - \langle t_{p,h} \rangle_h}{\sigma_p}, \langle t_{p,h} \rangle_h = \frac{\sum_h t_{p,h}}{\sum_h 1}, \sigma_p^2 = \langle t_{p,h}^2 \rangle_h - \langle t_{p,h} \rangle_h^2. \tag{7}$$

Here, the product of  $t'_{p,j}$  by its transpose  $t'_{p,i}{}^T$  results in the square matrix  $t''_{ij} = t'_{p,i}{}^T \cdot t'_{p,j}$ , and then its normalized matrix (called by a covariance correlation matrix)  $C_{ij}$  is defined by  $C_{ij} = t''_{ij} / \max\{t''_{ij}\}$ , where  $\max\{t''_{ij}\}$  is the maximum value of elements in the square matrix  $t''_{ij}$ . The larger the value of  $C_{ij}$ , the higher the covariance correlation between a subject  $i$  and a subject  $j$  in their profile of the cortical thickness at essential ROI vertices. Based on this covariance correlation matrix, we defined the severity degree AD for a given subject  $i$  by

$$SD_i = \left( \overline{C_i^{\text{AD-CN}}} - \overline{C_i^{\text{AD-CN}}}_{i \in \text{CN}} \right) / \left( \overline{C_i^{\text{AD-CN}}}_{i \in \text{AD}} - \overline{C_i^{\text{AD-CN}}}_{i \in \text{CN}} \right), \tag{8}$$

where  $\overline{C_i^{\text{AD-CN}}} = \langle C_{ij} \rangle_{j \in \text{AD}} - \langle C_{ij} \rangle_{j \in \text{CN}}$ . The severity degree of AD ranged from 0 for the basin of CN state to 1 for the basin of AD state. Rank-ordering this degree in ascending order illustrates that a subject  $i$  with the larger (or smaller) value of the severity degree is more prone to AD (CN) state.

**Results**

**Identification of essential ROI vertices at which the distributions of cortical thickness of CN, MCI, AD subjects are distinguishable**

Although the averaged cortical thickness of subjects with AD is generally known to be thinner than that of CN or MCI subjects, the distribution curves of averaged cortical thickness for the cohorts are not well distinguishable except near both ends of the distribution curves as demonstrated in Fig. 1A. This illustrates that a subject can be CN even

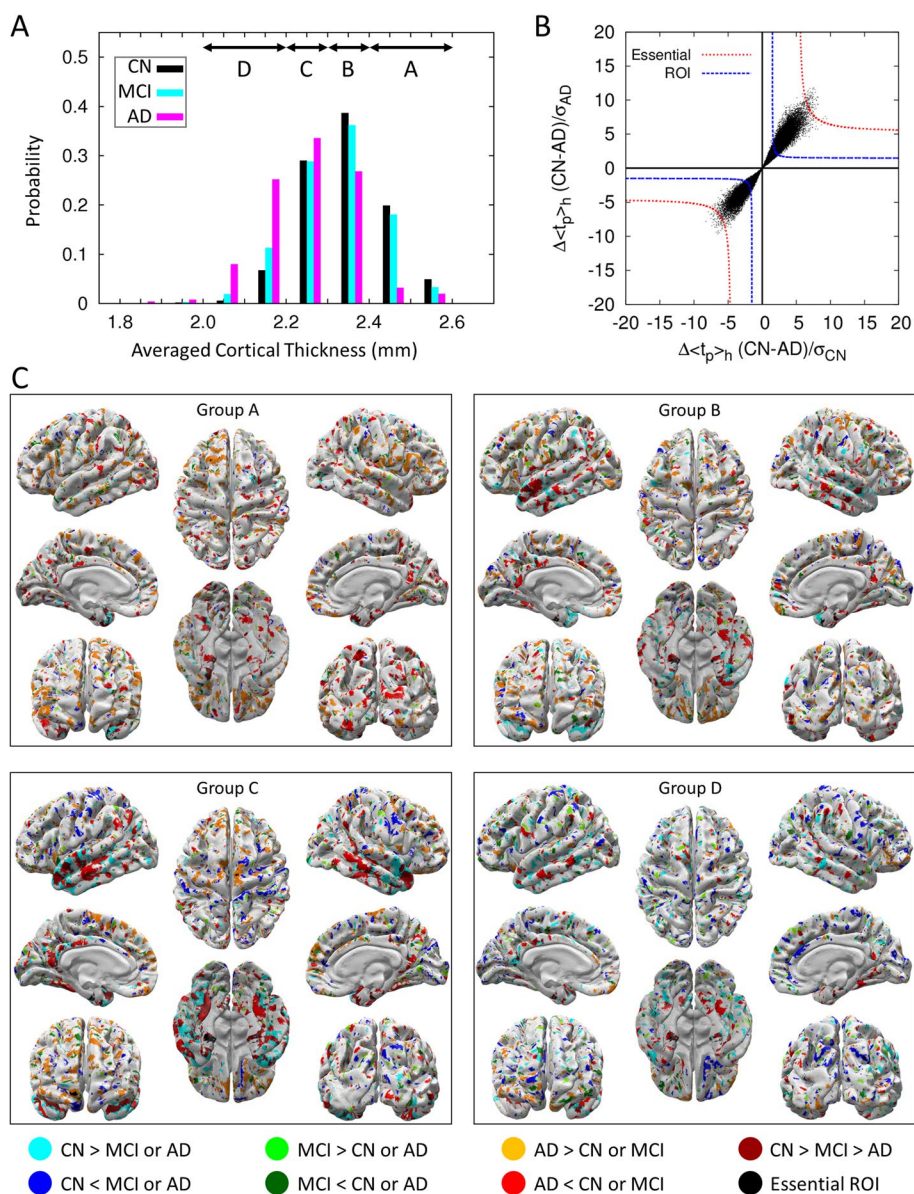


**Fig. 1** The classification of 1516 brain images into four groups by the average cortical thickness. **A** The distribution of average cortical thickness of subjects in the CN (black), MCI (cyan), and AD (magenta) cohorts. Above arrows point to the range of average cortical thickness. Subject number, sex, and age for each group are listed in Table 1. **B** For the cortical thickness group D, the degree of separation of the distribution curve of average cortical thickness between CN subjects and AD subjects is presented in the form of black points. The closer to the origin point (0, 0) the degree of separation of two distribution curves of average cortical thickness is, the less distinguishable they are (Additional file 1: Fig. S1). Black points residing outside of the blue-dashed line ( $Z = \pm 1.5$ ) are ROI vertices, and black points residing outside of red-dashed line ( $Z$  values are listed in Additional file 1: Table S1) are essential ROI vertices. **C** For each group of average cortical thickness, ROI vertices at which the thickness of the cortex for CN subjects is thicker (thinner) than that of the other subjects with MCI or AD is represented by cyan (blue) color. As a similar procedure, ROI vertices for MCI subjects is thicker (thinner) than the other cohorts is represented by green (dark green) color. Also, ROI vertices for AD subjects is thicker (thinner) than the other cohorts is represented by orange (red) color. Especially, the ROI vertices at which the cortical thickness decreases in the descending order of CN-MCI-AD is represented by dark red. And the essential ROI vertices are represented by a black color. The ROI vertices commonly found from more than three groups of average cortical thickness are presented in Additional file 1: Fig. S2, where it shows less congested and clear ROI vertices

though the averaged cortical thickness is thinner than that of a subject with AD, and vice versa. Also, we found that many subjects identified as CN, MCI, or AD have a similar averaged cortical thickness. This is due to the fact that the average cortical thickness for a subject was calculated over all 276,825 vertex points on the cortex, and the cortical thicknesses at most vertices are similar for all subjects, which prohibits us from successfully clustering 1552 human brain images into the image of CN, MCI, AD cohorts. Therefore, instead of resorting on the cortical thickness of all 276,825 vertex points on the cortex, we selected ROI vertices at which the cortical thickness values are distinguishable from each other among CN, MCI, and AD. For a fair selection of such ROI vertices, we divided the range of the averaged cortical thickness of subjects into four (A-D) different regions (for the detail, see the second section in methods).

Figure 1B illustrates how we identified ROI and essential ROI vertices. The x-axis  $(\langle t_{p,h \in \text{CN}} \rangle - \langle t_{p,h \in \text{AD}} \rangle) / \sqrt{\sigma_{p,h \in \text{CN}}^2 / n_{p,h \in \text{CN}}}$  represents the degree of separation between the distribution curves of cortical thickness for CN subjects and AD subjects at a vertex  $p$  normalized by the dispersion of the cortical thickness of CN subjects, which is quantified by the value of its  $Z$  score. The y-axis  $(\langle t_{p,h \in \text{CN}} \rangle - \langle t_{p,h \in \text{AD}} \rangle) / \sqrt{\sigma_{p,h \in \text{AD}}^2 / n_{p,h \in \text{AD}}}$  represents values normalized by the dispersion of the cortical thickness of individuals with AD. Therefore, the x-values (y-values) at a vertex point  $p$  represent the degree by which the distribution of cortical thickness at this point  $p$  of CN (AD) subjects is distinguished from averaged cortical thickness of subjects with AD (CN). It means the larger the value of  $(Z_p^{\text{CN-AD}})^2 = [x^{-2} + y^{-2}]^{-1}$  is, the two distribution curves are more distinguished each other (for the illustration, see Additional file 1: Fig. S1). The ROI cut-off line is defined by points satisfying  $|Z_p^{\text{CN-AD}}| = 1.5$ , and the distribution of cortical thickness of CN subjects and individuals with AD is clearly distinguished at those points satisfying  $|Z_p^{\text{CN-AD}}| > 1.5$  (outside of the ROI cut-off line).

Figure 1C shows ROI vertices for each of the cortical thickness groups (A-D) by colored points on the white cortex, at which the thickness of the cortex is either thicker or thinner particularly for one cohort compared with that of two other cohorts. These ROI vertices are widely distributed on the cortex, and their locations are not fixed but vary depending on the groups A to D. We uncovered, however, that the medial temporal lobe, known to be very important for memory formation, is always indicated by a red or dark red color irrespective of the groups A to D (Additional file 1: Fig. S2). This implies that the cortical thickness values of the medial temporal lobe for subjects with AD are characteristically thinner than those of CN subjects or individuals with MCI (red color), and this decrease occurs in the following descending order: CN-MCI- AD (dark red color). The medial temporal lobe is the region where the cortical thickness gradually decreases as AD severity increases and therefore is the critical region necessary for determining the AD cohort and the severity degree of AD. We also noted that the cortical thickness at the orange-colored region for subjects with AD is thicker than that for CN subjects or those with MCI. This has nothing to do with the damage in the cortex but contributes to the increase in the accuracy for predicting the AD cohort since it could provide better distinguishability of subjects with AD from CN subjects and those with MCI.

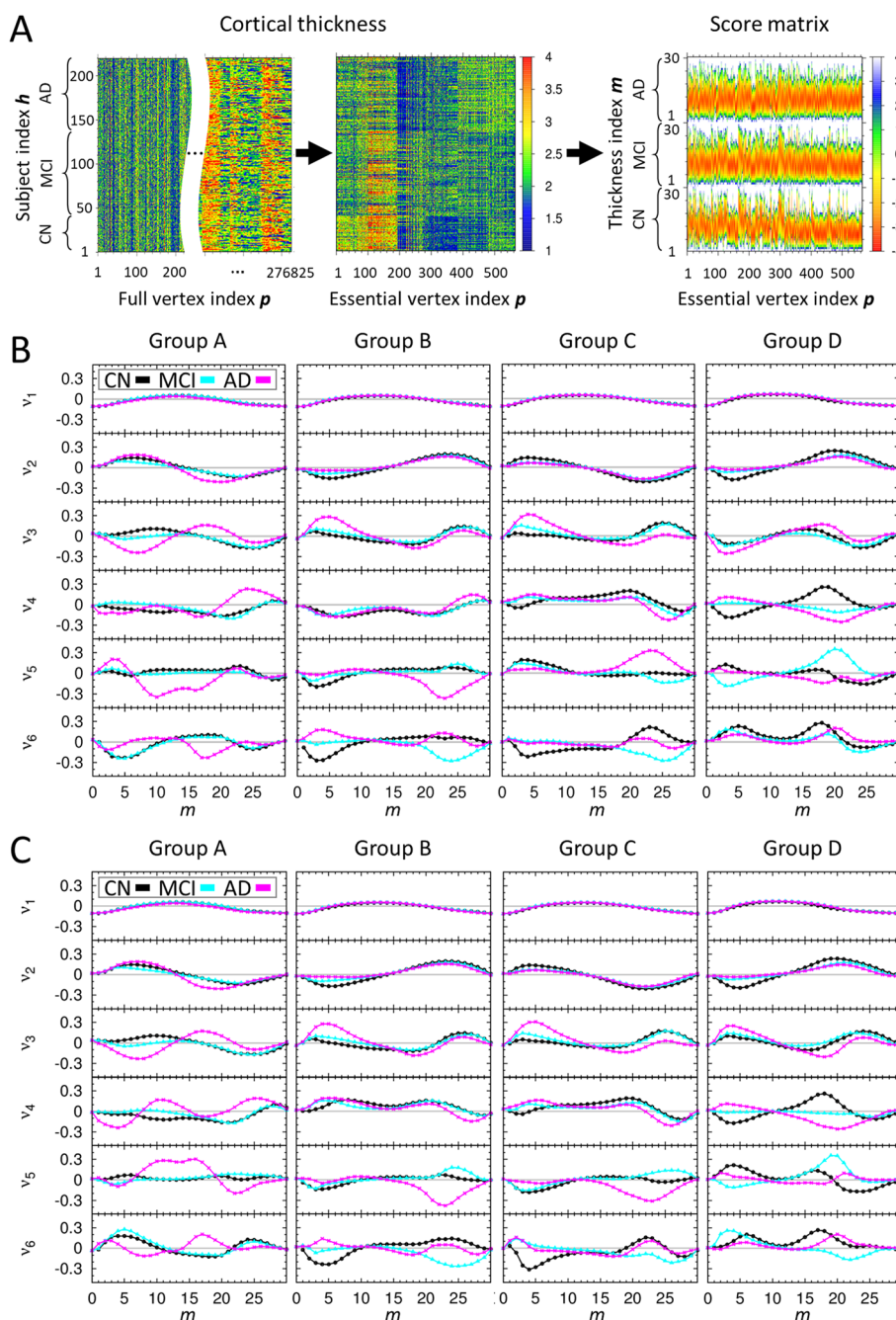


**Fig. 2** The character of score matrix for each group of average cortical thickness. **A** For a given group of average cortical thickness, three kinds of heat maps illustrate the process starting from the cortical thickness matrix at all 276,825 vertices to that at only 564 essential ROI vertices, and then construction of the score matrix. The dimension in the x-axis of the cortical thickness matrix at all 276,825 is too large to draw, we placed the blank in the middle to abbreviate the large dimension of the x-axis. **B** The results of singular value decomposition analysis on score matrices, which are composed of 547 CN, 722 MCI, 247 AD human brain images and used for self-recognition test. For each group of average cortical thickness, six singular vectors corresponding to the six largest singular values are presented. Here, x-axis is  $m$  value defined in the third section of methods, and y-axis is an arbitrary unit for the singular vectors. For each graph, the singular vector components for CN, MCI, and AD subjects are plotted by black, cyan, magenta colors, respectively. **C** The results of singular value decomposition analysis on score matrices, which are composed of 363 CN, 480 MCI, 163 AD human brain images as a training set and used for the first iteration of the stratified threefold cross validation test. The other results of that used for the second and third iterations of the stratified threefold cross validation test are presented in Additional file 1: Fig. S3

**Table 2** Result for the tests of the cohorts for each group

Exp	Group A			Group B			Group C			Group D			Correct	(%)
	CN	MCI	AD											
<i>Self-recognition test</i>														
CN	128	8	–	197	12	3	142	11	6	40	–	–	507	(92)
MCI	16	139	–	74	155	33	59	120	30	5	88	3	502	(69)
AD	–	–	13	6	1	60	7	2	75	1	3	79	227	(91)
<i>Stratified threefold cross validation test</i>														
CN	122	14	–	177	28	7	133	20	6	31	6	3	463	(84)
MCI	33	122	–	97	130	35	68	103	38	9	75	12	430	(59)
AD	1	–	12	5	9	53	7	11	66	2	8	73	204	(82)

“Exp” column, outside of the parenthesis, represents the number of MR images base on the clinical test, and “Score” row, inside of the parenthesis, represents the number of MR images base on our test using score matrix. AD, Alzheimer’s disease; CN, cognitively normal; MCI, mild cognitive impairment

**Character of statistical score matrix and classification of subject’s cohort**

The third section in methods described the detailed procedure of constructing the statistical score matrix for determining a subject’s cohort within each group of the average cortical thickness (Fig. 2A). In order to judge how well the statistical score matrix distinguishes CN, MCI, and AD cohorts from each other before we predict the cohort of a new subject, we performed the singular value decomposition (SVD) analysis on the combined statistical score matrix  $S^{(All)}$  which consists of matrix elements of  $S^{(CN)}$ ,  $S^{(MCI)}$ , and  $S^{(AD)}$ . We used the SVD character of a matrix that a given matrix can be reconstructed as a linear combination of the products of two singular vectors weighted by corresponding singular value. Since the reconstructed matrix from the few highest modes of singular values contains the predominant character of an original given matrix, one expects that the differences among the cohorts should appear in singular vectors of different cohorts. Otherwise, the statistical score matrix  $S^{(All)}$  is not reliable nor does it contain the characteristic ingredient of different cohorts. Figure 2B, C and Additional file 1: Fig. S3 show the highest six singular vectors corresponding to the six largest singular values from SVD analysis of the statistical score matrices for each group of the average cortical thickness A to D. Here, it demonstrates that elements in the singular vectors  $v_1$  to  $v_3$  for CN, MCI, and AD follow qualitatively a similar trend, meaning that these compose the fundamental default modes, whereas those in  $v_4$  to  $v_5$  follow a different trend and are distinguished each other.

Out of 547 CN, 722 MCI, and 247 AD human brain images provided from the ADNI data set and with their cohort predetermined clinically, we performed the self-recognition test and also the stratified threefold cross validation test for a cohort of subject using the 1516 human brain images for each group on the average cortical thickness A to D (Table 2 and Additional file 1: Table S2). For the first (second; third) iteration of stratified threefold cross validation test, 1006 (1011; 1015) human brain images were used as the training set for learning the statistical score matrix and 510 (505; 501) human brain images were used as an independent validation set. The new method presented in this study recognized and predicted the subjects with AD in the

cohort with more than 91% (self-recognition test) and 82% (stratified threefold cross validation test) accuracy, respectively.

There may be a problem that the demographics of the CN/MCI/AD cohort look quite different. Therefore, we performed statistical tests to check whether there are significant demographic differences between CN/MCI/AD cohorts. We checked through p-value whether the distribution of age within each group showed statistically significant differences (Additional file 1: Table S3). It can be said that there is no statistically significant difference because all p-values have values greater than 0.05. Since p-value cannot be calculated with respect to female percentage, we performed the reanalysis of the cortical thickness data by taking equal ratio between female and male in the demographics of the participants in Table 1. Even if the sex ratio was set to 1:1, our results were robust (Additional file 1: Table S4).

#### **Estimating the AD severity of subjects by a new predictor of covariance correlation matrix**

Developing a quantitative measure to tell the degree of AD severity for a given subject is very important for diagnosing and clinically treating patients with MCI and AD with the different degree of AD. In this study, we already identified essential ROI vertices and constructed the statistical score matrices as an initial classifier ensuring the prediction of subjects with AD at more than 80% accuracy that they belong to the AD cohort. Thus, we extracted the cortical thickness profile (or vector) at essential ROI vertices for all brain images, and constructed the covariance correlation matrix between them. Then we calculated the correlation between the profile vector for a given subject's image with that of patients with AD, to estimate the degree of AD severity for a given subject relative to patients with AD (for the detail, see the Eq. (8) in the fourth section in methods and Fig. 3A). The personalized and quantitative severity degree of AD (the Eq. (8)) is plotted at the right-bottom graph of Fig. 3A for each subject of CN, MCI, AD cohort of the group D in the ascending order. The values of severity degree of AD were distributed around the averaged value of 0 (ranging from about -0.5 to +0.5) for subjects with CN, 0.5 (ranging from about -0.2 to +1.2) for subjects with MCI, and 1.0 (ranging from about +0.2 to +1.5) for subjects with AD, respectively. The distribution of the severity degree for subjects with MCI was laid across both ranges of those for CN and AD, which points out that this is the intrinsic source of the low success ratio in determining the AD cohort of subjects with MCI. One could unfold and sort out quantitatively the broad spectrum of the AD severity for MCI subjects in that whether they are prone to CN or AD. Given a new person for diagnosing the AD state, one of the cohort CN, MCI, AD was assigned by the Eq. (3) and the personalized and quantitative severity degree of AD was estimated by the Eq. (8). Then, with these two qualitative- and quantitative-determinants, one may infer that a new person with the estimated severity degree below 0.0 is most likely to be CN, with that between 0.0 and 0.5 might be CN or MCI prone to CN, with that between 0.5 and 1.0 might be MCI prone to AD or AD, and with that above 1.0 is most likely to be AD state.

We constructed the covariance correlation matrices for all groups A, B, C, D of the average cortical thickness and observed the common pattern in the matrices that subjects with AD (CN), possessing a strong correlation among themselves are clustered

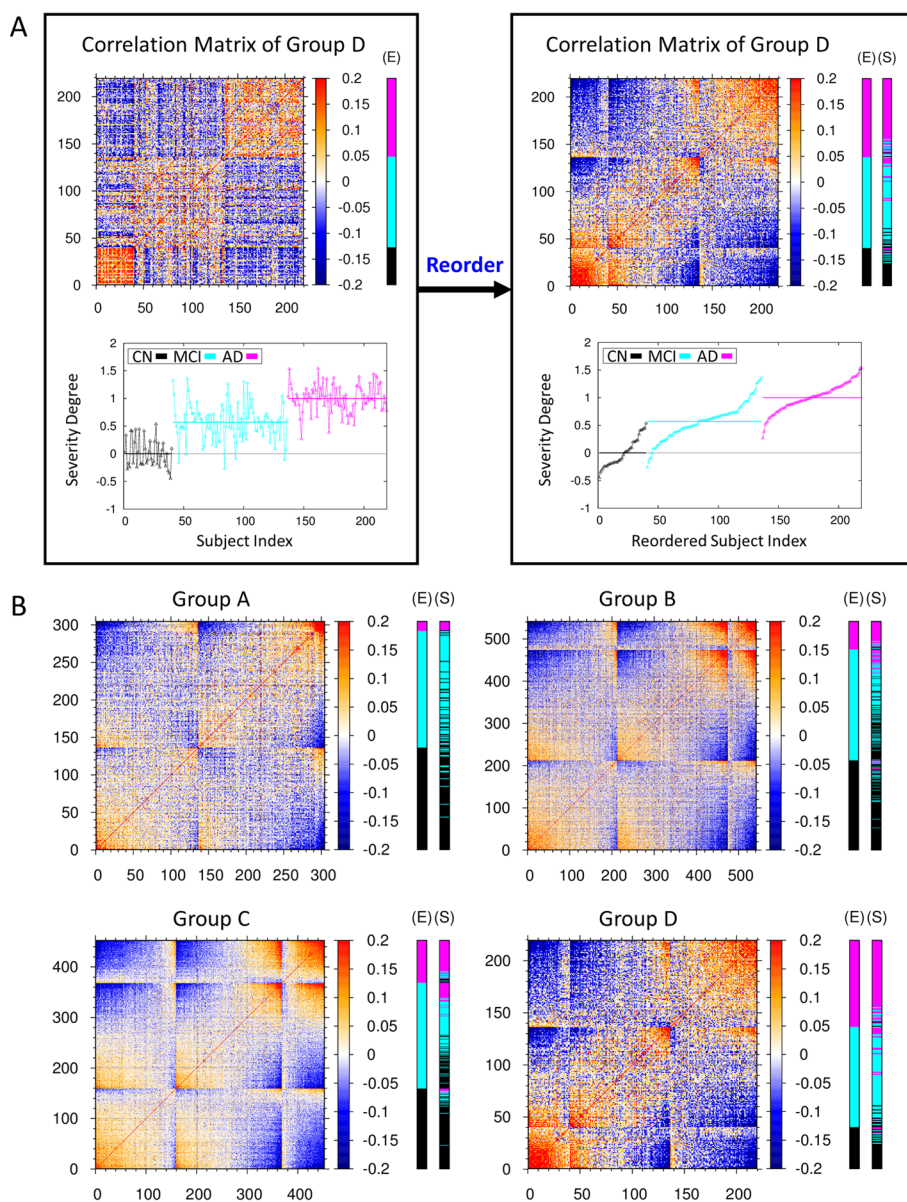


**Fig. 3** Covariance correlation matrix and severity degree of AD. **A** The left-top heat map is the covariance correlation matrix for group D of average cortical thickness. The x- and y-axes represent the indices 1 to 40 for CN subjects, 41 to 136 for MCI subjects, and 137 to 219 for AD subjects. Here, red (blue) color represents the high (low) correlation between two subjects at the essential ROI vertices. The extra E-cohort color bar at the right of the heat map represents the clinically determined cohort of CN subjects and subjects with MCI and AD denoted by black, cyan, and magenta colors, respectively. The left-bottom graph illustrates the personalized severity degree of AD for each subjects of the group D in terms of a quantitative value, ranging from 0 for the basin of CN state to 1 for the basin of AD state (for the detail, see the fourth section in methods). The average values of this severity degree in each cohort are denoted by horizontal lines, respectively. The left panel is reordered into the right panel according to the ascending value of the severity degree in each cohort. For those subjects with MCI, the distribution of severity degree of AD is very broad. One can sort out the broad spectrum of the AD severity for MCI subjects in that whether they are prone to CN or how much they are progressed toward AD. **B** The reordered covariance correlation matrices for A, B, C, and D groups of average cortical thickness together with the determination of CN (black), MCI (cyan), and AD (magenta) cohorts by clinical (E-cohort color bar) exam and by the stratified threefold cross validation test of this study (S-cohort color bar). The original covariance correlation matrices for the four groups of average cortical thickness are provided in Additional file 1: Fig. S4

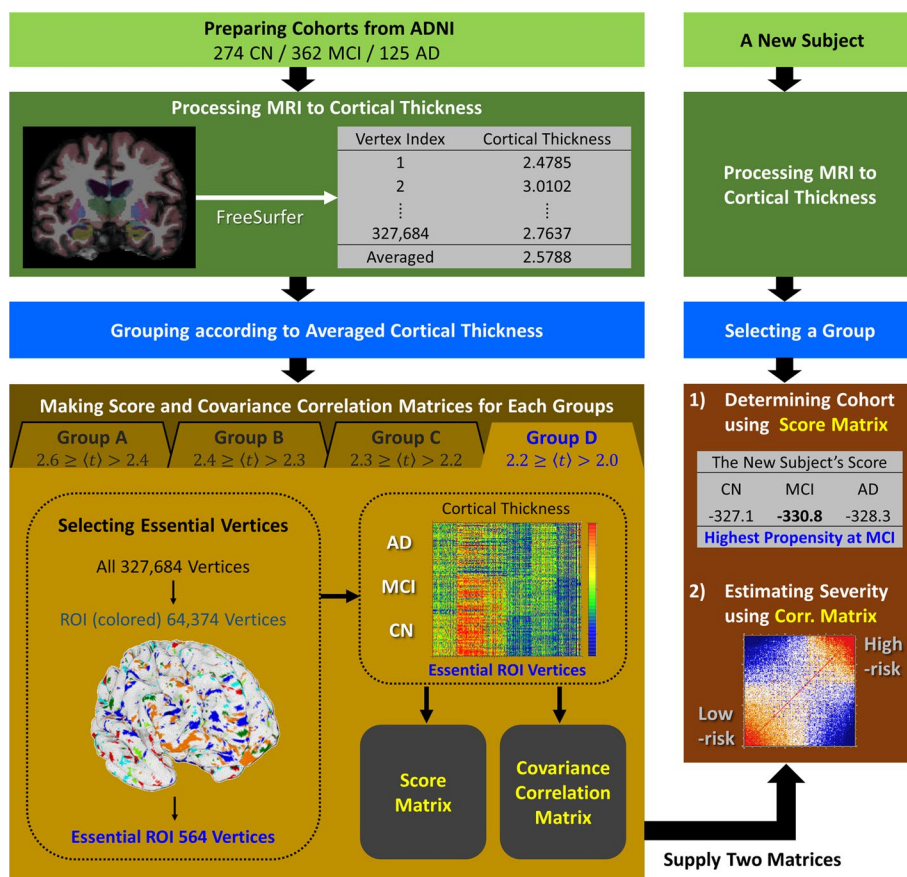


**Fig. 4** Flow chart for the cohort determination and the estimation of the severity degree of AD. The left shows the process of constructing the score matrix and covariance correlation matrix from the cortical thickness big data of subjects derived from the ADNI data set. The right shows the process of determining the cohort and the severity degree of AD for a new given subject

at the top-right (bottom-left) corner, represented by the cluster of red colors (Additional file 1: Fig. S4). Also, we presented the reordered covariance correlation matrices by the severity degree of AD and the results to which one of the CN, MCI, AD cohorts each human brain would belong, based on both the clinical test and our stratified threefold cross validation test (Fig. 3B). After comparing the result from our independent validation test with that of the clinical test, we noted that those subjects which were predicted to belong to the MCI cohort by the clinical test and yet estimated to have the higher (lower) severity degree of AD by our estimation, were predicted to belong to the AD (CN) cohort from the our validation test.

### Discussion

Based on the cortical thickness data of 1516 human brain images from the ADNI data set, we presented a new algebraic determinant for both (1) the identification of the cohort (CN, MCI, AD) a given subject would belong to and (2) the quantitative estimation of the severity degree of AD for a given new person (Fig. 4). A total of 1516 human brain MR images were partitioned into four groups by the average cortical

thickness of each subject. Out of 327,684 vertices on the cortex, a few hundred essential ROI vertices for each group were identified, which were enough to distinguish the cortical thickness distribution of the CN, MCI, and AD cohorts from each other. Statistical score matrices using the cortical thickness on the essential ROI vertices were constructed as an initial classifier for determining the cohort of a given subject. Out of 547 CN, 722 MCI, and 247 AD subjects predetermined clinically, the success ratio for self-recognizing their cohort was 92% with CN, 69% with MCI, and 91% with AD subjects. On the other hand, employing 1006 human brain images for control and 510 human brain images for independent validation, the stratified threefold cross-validation test gave the correct prediction rate of 84% with CN, 59% with MCI, and 82% in subjects with AD; this is in the overall agreement with the results of clinical determination. Using the quantitative severity degree of AD for subjects, we could explain the reason why the inevitable uncertainty in the determination of the MCI cohort arose by the very broad distribution of the severity degree of AD which MCI subjects possess intrinsically. We suggested that the severity degree of AD presented in this study would be a realistic measure for the quantitative and personalized diagnosis of a given subject instead of tri-partitioning the classification of a subject's cohort only by CN, MCI or AD. It is the continuous degree of AD severity for a given subject along the scale from 0 for the basin of CN state to 1 for the basin of AD state. One could sort out quantitatively the broad spectrum of the severity degree of AD for MCI or AD subjects with the different severity degree in that whether they are prone to CN or how much they are progressed toward AD.

### Limitations

We noted above that the correct prediction rate of cohort for MCI subjects is 59% which is lower than 84%, 82% for CN and AD subjects, respectively. This is because, as represented in Additional file 1: Fig. S2, there are no particular cortex regions in a brain, at which the cortical thickness is markedly different for MCI subjects compared to those for CN and AD subjects. Despite of such difficulties in predicting the cohort of subjects with MCI, we introduced a new quantitative determinant “the severity degree of AD” so that we could identify MCI state by the quantitative manner as an intermediate one between CN and AD states (Fig. 3A). Therefore, instead of trying to single out MCI state as the one which is distinctively distinguished from CN and AD states, we focused on accessing how much a given subject with MCI possesses the similar character with that of subjects with AD. Our ultimate mission in the future would be to verify how much the severity degree of AD for subjects with MCI will be correlated with the occurrence rate of AD in a longitudinal study.

### Conclusions

This study not only provided a straightforward algebraic determinant to analyzing the cortical thicknesses of human brains but also suggested quantitative measures by which one could estimate both the cohort and the severity degree of AD for a given new subject based on the neuro-images from the structural MRI. The MRI data of a larger number of human

brains could also be implemented into this study in a systematic and robust manner, which would facilitate the better diagnose of AD with the different degree of dementia.

## Supplementary Information

The online version contains supplementary material available at <https://doi.org/10.1186/s12859-022-04903-8>.

**Additional file 1:** Supplementary Figures and Tables.

## Acknowledgements

National Research Foundation (2017R1E1A1A03070854), Korea. We acknowledged DGIST supercomputing big data center for the allocation of supercomputing resources. We appreciated Mookyung Cheon and Wookyung Yu for the fruitful discussions, and also Keonho Lee and Jangjae Lee of Chosun University for the preparation of MRI image data in the initial stage of this work.

## The Alzheimer's Disease Neuroimaging Initiative

Lisa C. Silbert<sup>5</sup>, Betty Lind<sup>5</sup>, Rachel Crissey<sup>7</sup>, Lon S. Schneider<sup>6</sup>, Sonia Pawluczuk<sup>6</sup>, Mauricio Becerra<sup>6</sup>, Liberty Teodoro<sup>6</sup>, Karen Dagerman<sup>6</sup>, James Brewer<sup>7</sup>, Helen Vanderswag<sup>7</sup>, Jaimie Ziolkowski<sup>8</sup>, Judith L. Heidebrink<sup>8</sup>, Lisa Zbizek-Nulph<sup>8</sup>, Lisa Zbizek-Nulph<sup>8</sup>, Ronald Petersen<sup>9</sup>, Sara S. Mason<sup>9</sup>, Colleen S. Albers<sup>9</sup>, David Knopman<sup>9</sup>, Kris Johnson<sup>9</sup>, Javier Villanueva-Meyer<sup>10</sup>, Valory Pavlik<sup>10</sup>, Nathaniel Pacini<sup>10</sup>, Ashley Lamb<sup>10</sup>, Joseph S. Kass<sup>10</sup>, Yaakov Stern<sup>11</sup>, Lawrence S. Honig<sup>11</sup>, Akiva Mintz<sup>11</sup>, Beau Ances<sup>12</sup>, John C. Morris<sup>12</sup>, David Winkfield<sup>12</sup>, Maria Carroll<sup>12</sup>, David Geldmacher<sup>13</sup>, Marissa Natelson Love<sup>13</sup>, Hillel Grossman<sup>14</sup>, Martin A. Goldstein<sup>14</sup>, Jonathan Greenberg<sup>14</sup>, Raj C. Shah<sup>15</sup>, Melissa Lamar<sup>15</sup>, Patricia Samuels<sup>15</sup>, Ranjan Duara<sup>16</sup>, Maria T. Greig-Custo<sup>16</sup>, Rosemarie Rodriguez<sup>16</sup>, Marilyn Albert<sup>17</sup>, Chiadi Onyike<sup>17</sup>, Leonie Farrington<sup>17</sup>, Scott Rudow<sup>17</sup>, Rottislav Brichko<sup>17</sup>, Amanda Smith<sup>18</sup>, Martin Sadowski<sup>19</sup>, Thomas Wisniewski<sup>19</sup>, Melanie Shulman<sup>19</sup>, Arline Faustin<sup>19</sup>, Julia Rao<sup>19</sup>, Karen M. Castro<sup>19</sup>, Anasztasia Ulysse<sup>19</sup>, Shannon Chen<sup>19</sup>, P. Murali Doraiswamy<sup>20</sup>, Jeffrey R. Petrella<sup>20</sup>, Olga James<sup>20</sup>, Terence Z. Wong<sup>20</sup>, Jason H. Karlawish<sup>21</sup>, David A. Wolk<sup>21</sup>, Sanjeev Vaishnavi<sup>21</sup>, Charles D. Smith<sup>22</sup>, Gregory A. Jicha<sup>22</sup>, Riham El Khoulil<sup>22</sup>, Flavius D. Raslau<sup>22</sup>, Oscar L. Lopez<sup>23</sup>, MaryAnn Oakley<sup>23</sup>, Donna M. Simpson<sup>23</sup>, Anton P. Porsteinsson<sup>24</sup>, Kim Martin<sup>24</sup>, Nancy Kowalski<sup>24</sup>, Melanie Keltz<sup>24</sup>, Gaby Thai<sup>25</sup>, Aimee Pierce<sup>25</sup>, Beatriz Yanez<sup>25</sup>, Elizabeth Sosa<sup>25</sup>, Megan Witbracht<sup>25</sup>, Brendan Kelley<sup>26</sup>, Trung Nguyen<sup>26</sup>, Kyle Womack<sup>26</sup>, Allan I. Levey<sup>27</sup>, James J. Lah<sup>27</sup>, Ihab Hajjar<sup>27</sup>, Jeffrey M. Burns<sup>28</sup>, Russell H. Swerdlow<sup>28</sup>, William M. Brooks<sup>28</sup>, Daniel H.S. Silverman<sup>29</sup>, Sarah Kremen<sup>29</sup>, Neill R. Graff-Radford<sup>30</sup>, Francine Parfitt<sup>30</sup>, Kim Poki-Walker<sup>30</sup>, Martin R. Farlow<sup>31</sup>, Jared R. Brosch<sup>31</sup>, Scott Herring<sup>31</sup>, Christopher H. van Dyc<sup>32</sup>, Adam P. Mecca<sup>32</sup>, Susan P. Good<sup>32</sup>, Martha G. MacAvoy<sup>32</sup>, Richard E. Carson<sup>32</sup>, Pradeep Varma<sup>32</sup>, Howard Chertkow<sup>33</sup>, Susan Vaitekunis<sup>33</sup>, Chris Hosein<sup>33</sup>, Sandra Black<sup>34</sup>, Bojana Stefanovic<sup>34</sup>, Chris (Chinthaka) Heyn<sup>34</sup>, Ging-Yuek Robin Hsiung<sup>35</sup>, Ellen Kim<sup>35</sup>, Benita Mudge<sup>35</sup>, Vesna Sossi<sup>35</sup>, Elizabeth Finger<sup>36</sup>, Stephen Pasternak<sup>36</sup>, Irina Rachinsky<sup>36</sup>, Ian Grant<sup>37</sup>, Brittanie Muse<sup>37</sup>, Emily Rogalski<sup>37</sup>, Jordan Robson<sup>37</sup>, Nunzio Pomara<sup>38</sup>, Raymundo Hernandez<sup>38</sup>, Antero Sarraeal<sup>38</sup>, Howard J. Rosen<sup>39</sup>, Bruce L. Miller<sup>39</sup>, David Perry<sup>39</sup>, Raymond Scott Turner<sup>40</sup>, Kathleen Johnson<sup>40</sup>, Brigid Reynolds<sup>40</sup>, Kelly McCann<sup>40</sup>, Jessica Poe<sup>40</sup>, Reisa A. Sperling<sup>41</sup>, Keith A. Johnson<sup>41</sup>, Gad A. Marshall<sup>41</sup>, Jerome Yesavage<sup>42</sup>, Joy L. Taylor<sup>42</sup>, Steven Chao<sup>42</sup>, Jaila Coleman<sup>42</sup>, Christine M. Belden<sup>43</sup>, Alireza Atri<sup>43</sup>, Bryan M. Spann<sup>43</sup>, Kelly A. Clark<sup>43</sup>, Ronald Killiany<sup>44</sup>, Robert Stern<sup>44</sup>, Jesse Mez<sup>44</sup>, Thomas O. Obisesan<sup>45</sup>, Oyonomo E. Ntekim<sup>45</sup>, Saba Wolday<sup>45</sup>, Javed I. Khan<sup>45</sup>, Evaristus Nwulia<sup>45</sup>, Sheeba Nadarajah<sup>45</sup>, Alan Lerner<sup>46</sup>, Paula Ogrocki<sup>46</sup>, Curtis Tatsuoka<sup>46</sup>, Parianne Fatica<sup>46</sup>, Evan Fletcher<sup>47</sup>, Pauline Maillard<sup>47</sup>, John Olichney<sup>47</sup>, Charles DeCarli<sup>47</sup>, Vernice Bates<sup>48</sup>, Horacio Capote<sup>48</sup>, Michelle Rainka<sup>48</sup>, Michael Borrie<sup>49</sup>, T-Y Lee<sup>49</sup>, Rob Bartha<sup>49</sup>, Sterling Johnson<sup>50</sup>, Sanjay Asthana<sup>50</sup>, Cynthia M. Carlsson<sup>50</sup>, Allison Perrin<sup>51</sup>, Douglas W. Scharre<sup>52</sup>, Maria Katakis<sup>52</sup>, Rawan Tarawneh<sup>52</sup>, David Hart<sup>53</sup>, Earl A. Zimmerman<sup>53</sup>, Dzintra Celmins<sup>53</sup>, Delwyn D. Miller<sup>54</sup>, Laura L. Boles Ponto<sup>54</sup>, Karen Ekstam Smith<sup>54</sup>, Hristina Koleva<sup>54</sup>, Hyungsub Shim<sup>54</sup>, Jeff D. Williamson<sup>55</sup>, Suzanne Craft<sup>55</sup>, Jo Cleveland<sup>55</sup>, Brian R. Ott<sup>56</sup>, Jonathan Drake<sup>56</sup>, Geoffrey Tremont<sup>56</sup>, Lori A. Daiello<sup>56</sup>, Jonathan D. Drake<sup>56</sup>, Marwan Sabbagh<sup>57</sup>, Aaron Ritter<sup>57</sup>, Abigail O'Connell<sup>58</sup>, Jacobo Mintzer<sup>58</sup>, Arthur Williams<sup>58</sup>, Joseph Masdeu<sup>59</sup>, Jiong Shi<sup>60</sup>, Angelica Garcia<sup>60</sup>, Paul Newhouse<sup>61</sup>, Steven Potkin<sup>62</sup>, Stephen Salloway<sup>63</sup>, Paul Malloy<sup>63</sup>, Stephen Correia<sup>63</sup>, Athena Lee<sup>64</sup>.

<sup>5</sup>Oregon Health & Science University. <sup>6</sup>University of Southern California. <sup>7</sup>University of California – San Diego. <sup>8</sup>University of Michigan. <sup>9</sup>Mayo Clinic, Rochester. <sup>10</sup>Baylor College of Medicine. <sup>11</sup>Columbia University Medical Center. <sup>12</sup>Washington University, St. Louis. <sup>13</sup>University of Alabama—Birmingham. <sup>14</sup>Mount Sinai School of Medicine. <sup>15</sup>Rush University Medical Center. <sup>16</sup>Wien Center. <sup>17</sup>Johns Hopkins University. <sup>18</sup>University of South Florida: USF Health Byrd Alzheimer's Institute. <sup>19</sup>New York University. <sup>20</sup>Duke University Medical Center. <sup>21</sup>University of Pennsylvania. <sup>22</sup>University of Kentucky. <sup>23</sup>University of Pittsburgh. <sup>24</sup>University of Rochester Medical Center. <sup>25</sup>University of California Irvine IMIND. <sup>26</sup>University of Texas Southwestern Medical School. <sup>27</sup>Emory University. <sup>28</sup>University of Kansas, Medical Center. <sup>29</sup>University of California, Los Angeles. <sup>30</sup>Mayo Clinic, Jacksonville. <sup>31</sup>Indiana University. <sup>32</sup>Yale University School of Medicine. <sup>33</sup>McGill Univ., Montreal-Jewish General Hospital. <sup>34</sup>Sunnybrook Health Sciences, Ontario. <sup>35</sup>U.B.C. Clinic for AD & Related Disorders. <sup>36</sup>St. Joseph's Health Care. <sup>37</sup>Northwestern University. <sup>38</sup>Nathan Kline Institute. <sup>39</sup>University of California, San Francisco. <sup>40</sup>Georgetown University Medical Center. <sup>41</sup>Brigham and Women's Hospital. <sup>42</sup>Stanford University. <sup>43</sup>Banner Sun Health Research Institute. <sup>44</sup>Boston University. <sup>45</sup>Howard University. <sup>46</sup>Case Western Reserve University. <sup>47</sup>University of California, Davis – Sacramento. <sup>48</sup>Dent Neurologic Institute. <sup>49</sup>Parkwood Institute. <sup>50</sup>University of Wisconsin. <sup>51</sup>Banner Alzheimer's Institute. <sup>52</sup>Ohio State University. <sup>53</sup>Albany Medical College. <sup>54</sup>University of Iowa College of Medicine. <sup>55</sup>Wake Forest University Health Sciences. <sup>56</sup>Rhode Island Hospital. <sup>57</sup>Cleveland Clinic Lou Ruvo Center for Brain Health. <sup>58</sup>Roper St. Francis Health-care. <sup>59</sup>Houston Methodist Neurological Institute. <sup>60</sup>Barrow Neurological Institute. <sup>61</sup>Vanderbilt University Medical Center. <sup>62</sup>Long Beach VA Neuropsychiatric Research Program. <sup>63</sup>Butler Hospital Memory and Aging Program. <sup>64</sup>Cornell University. Data used in preparation of this article were obtained from the Alzheimer's Disease Neuroimaging Initiative (ADNI) database ([adni.loni.usc.edu](http://adni.loni.usc.edu)). As such, the investigators within the ADNI contributed to the design and implementation of ADNI and/or provided data but did not participate in analysis or writing of this report. A complete listing of ADNI investigators can be found at: [http://adni.loni.usc.edu/wp-content/uploads/how\\_to\\_apply/ADNI\\_Acknowledgement\\_List.pdf](http://adni.loni.usc.edu/wp-content/uploads/how_to_apply/ADNI_Acknowledgement_List.pdf).

**Author contributions**

The research planning was conceived by SK and IC. The processing of MRI image data from ADNI and the evaluation of cortical thickness of human brains were done by SP and SK. The statistically learned score matrix and a covariance matrix as a set of classifier and predictor were constructed by SK and IC. The in-depth interpretation of data, manuscript writing were done by all authors. All authors read and approved the final manuscript.

**Funding**

National Research Foundation (2017R1E1A1A03070854), Korea.

**Availability of data and materials**

Data used in the preparation of this article were obtained from the Alzheimer's Disease Neuroimaging Initiative (ADNI) database ([adni.loni.usc.edu](http://adni.loni.usc.edu)). The ADNI was launched in 2003 as a public–private partnership, led by principal investigator Michael W. Weiner, MD. The primary goal of the ADNI has been to test whether serial MRI, PET, other biological markers, and clinical and neuropsychological assessment can be combined to measure the progression of MCI and early Alzheimer's disease. For up-to-date information, see [www.adni-info.org](http://www.adni-info.org). Data collection and sharing for this project was funded by the AD Neuroimaging Initiative (ADNI) (National Institutes of Health Grant U01 AG024904) and DOD ADNI (Department of Defense award number W81XWH-12-2-0012). ADNI is funded by the National Institute on Aging, the National Institute of Biomedical Imaging and Bioengineering, and through generous contributions from the following: AbbVie, Alzheimer's Association; Alzheimer's Drug Discovery Foundation; Araclon Biotech; BioClinica, Inc.; Biogen; Bristol-Myers Squibb Company; CereSpir, Inc.; Cogstate; Eisai Inc.; Elan Pharmaceuticals, Inc.; Eli Lilly and Company; EuroImmun; F. Hoffmann-La Roche Ltd and its affiliated company Genentech, Inc.; Fujirebio; GE Healthcare; IXICO Ltd.; Janssen Alzheimer Immunotherapy Research & Development, LLC.; Johnson & Johnson Pharmaceutical Research & Development LLC.; Lumosity; Lundbeck; Merck & Co., Inc.; Meso Scale Diagnostics, LLC.; NeuroRx Research; Neurotrack Technologies; Novartis Pharmaceuticals Corporation; Pfizer Inc.; Piramal Imaging; Servier; Takeda Pharmaceutical Company; and Transition Therapeutics. The Canadian Institutes of Health Research is providing funds to support ADNI clinical sites in Canada. Private sector contributions are facilitated by the Foundation for the National Institutes of Health ([www.fnih.org](http://www.fnih.org)). The grantee organization is the Northern California Institute for Research and Education, and the study is coordinated by the Alzheimer's Therapeutic Research Institute at the University of Southern California. ADNI data are disseminated by the Laboratory for Neuro Imaging at the University of Southern California.

**Declarations****Ethics approval and consent to participate**

Not applicable.

**Consent for publication**

Not applicable.

**Competing interests**

The authors declare no competing interests.

Received: 21 March 2022 Accepted: 24 August 2022

Published online: 29 August 2022

**References**

- Galvin JE, Sadowsky CH, Nincds A. Practical guidelines for the recognition and diagnosis of dementia. *J Am Board Family Med: JABFM*. 2012;25(3):367–82.
- Solomon A, Soininen H. Dementia: Risk prediction models in dementia prevention. *Nat Rev Neurol*. 2015;11(7):375–7.
- Raj A, Kuceyeski A, Weiner M. A network diffusion model of disease progression in dementia. *Neuron*. 2012;73(6):1204–15.
- Coughlan G, Coutrot A, Khondoker M, Minihane AM, Spiers H, Hornberger M. Toward personalized cognitive diagnostics of at-genetic-risk Alzheimer's disease. *Proc Natl Acad Sci USA*. 2019;116(19):9285–92.
- Wang J, Knol MJ, Tulpin A, Dubost F, de Bruijne M, Vernooij MW, et al. Gray matter age prediction as a biomarker for risk of dementia. *Proc Natl Acad Sci USA*. 2019;116(42):21213–8.
- Hojjati SH, Ebrahimzadeh A, Babajani-Feremi A. Identification of the early stage of Alzheimer's disease using structural MRI and resting-state fMRI. *Front Neurol*. 2019;10:904.
- Kim BH, Choi YH, Yang JJ, Kim S, Nho K, Lee JM, et al. Identification of novel genes associated with cortical thickness in Alzheimer's disease: systems biology approach to neuroimaging endophenotype. *J Alzheimer's Dis: JAD*. 2020;75(2):531–45.
- Qiu S, Joshi PS, Miller MI, Xue C, Zhou X, Karjadi C, et al. Development and validation of an interpretable deep learning framework for Alzheimer's disease classification. *Brain: J Neurol*. 2020;143(6):1920–33.
- Tetreault AM, Phan T, Orlando D, Lyu I, Kang H, Landman B, et al. Network localization of clinical, cognitive, and neuropsychiatric symptoms in Alzheimer's disease. *Brain: J Neurol*. 2020;143(4):1249–60.
- Reber J, Hwang K, Bowren M, Bruss J, Mukherjee P, Tranel D, et al. Cognitive impairment after focal brain lesions is better predicted by damage to structural than functional network hubs. *Proc Natl Acad Sci USA*. 2021;118(19):e2018784118.
- Zhang X, Mormino EC, Sun N, Sperling RA, Sabuncu MR, Yeo BT, et al. Bayesian model reveals latent atrophy factors with dissociable cognitive trajectories in Alzheimer's disease. *Proc Natl Acad Sci USA*. 2016;113(42):E6535–44.

12. Hartikainen P, Rasanen J, Julkunen V, Niskanen E, Hallikainen M, Kivipelto M, et al. Cortical thickness in frontotemporal dementia, mild cognitive impairment, and Alzheimer's disease. *J Alzheimer's Dis: JAD*. 2012;30(4):857–74.
13. Im K, Lee JM, Seo SW, Yoon U, Kim ST, Kim YH, et al. Variations in cortical thickness with dementia severity in Alzheimer's disease. *Neurosci Lett*. 2008;436(2):227–31.
14. Kim HJ, Ye BS, Yoon CW, Noh Y, Kim GH, Cho H, et al. Cortical thickness and hippocampal shape in pure vascular mild cognitive impairment and dementia of subcortical type. *Eur J Neurol*. 2014;21(5):744–51.
15. Lebedev AV, Westman E, Beyer MK, Kramberger MG, Aguilar C, Pirtosek Z, et al. Multivariate classification of patients with Alzheimer's and dementia with Lewy bodies using high-dimensional cortical thickness measurements: an MRI surface-based morphometric study. *J Neurol*. 2013;260(4):1104–15.
16. Paternico D, Manes M, Premi E, Cosseddu M, Gazzina S, Alberici A, et al. Frontotemporal dementia and language networks: cortical thickness reduction is driven by dyslexia susceptibility genes. *Sci Rep*. 2016;6:30848.
17. Querbes O, Aubry F, Pariente J, Lotterie JA, Demonet JF, Duret V, et al. Early diagnosis of Alzheimer's disease using cortical thickness: impact of cognitive reserve. *Brain: J Neurol*. 2009;132(Pt 8):2036–47.
18. Saleem TJ, Zahra SR, Wu F, Alwakeel A, Alwakeel M, Jeribi F, et al. Deep learning-based diagnosis of Alzheimer's disease. *J Personal Med*. 2022;12(5):815.
19. Raju M, Gopi VP, Anitha VS, Wahid KA. Multi-class diagnosis of Alzheimer's disease using cascaded three dimensional-convolutional neural network. *Phys Eng Sci Med*. 2020;43(4):1219–28.
20. Albright J. Forecasting the progression of Alzheimer's disease using neural networks and a novel preprocessing algorithm. *Alzheimers Dement*. 2019;5:483–91.
21. Dale AM, Fischl B, Sereno MI. Cortical surface-based analysis. I Segmentation and surface reconstruction. *Neuroimage*. 1999;9(2):179–94.
22. Fischl B, Sereno MI, Dale AM. Cortical surface-based analysis. II: Inflation, flattening, and a surface-based coordinate system. *Neuroimage*. 1999;9(2):195–207.
23. Yu W, Lee W, Lee W, Kim S, Chang I. Uncovering symmetry-breaking vector and reliability order for assigning secondary structures of proteins from atomic NMR chemical shifts in amino acids. *J Biomol NMR*. 2011;51(4):411–24.

### Publisher's Note

Springer Nature remains neutral with regard to jurisdictional claims in published maps and institutional affiliations.

**Ready to submit your research? Choose BMC and benefit from:**

- fast, convenient online submission
- thorough peer review by experienced researchers in your field
- rapid publication on acceptance
- support for research data, including large and complex data types
- gold Open Access which fosters wider collaboration and increased citations
- maximum visibility for your research: over 100M website views per year

**At BMC, research is always in progress.**

Learn more [biomedcentral.com/submissions](https://biomedcentral.com/submissions)

